Proceedings of Global Power and Propulsion Society
ISSN-Nr: 2504-4400
GPPS Xi'an21
18th – 20th October, 2021
www.gpps.global

GPPS-TC-2021-0171

EFFECTS OF FILM HOLE DIAMETER AND WALL THICKNESS ON OVERALL COOLING EFFECTIVENESS OF TURBINE VANE LEADING EDGE

Rui Wang
Northwestern Polytechnical University
wr1888590@163.com
Xi'an, Shaanxi, China

Cun-liang Liu
Northwestern Polytechnical University
liucunliang@nwpu.edu.cn
Xi'an, Shaanxi, China

Qi-hao Chen
Northwestern Polytechnical University
qihaox_chen@163.com
Xi'an, Shaanxi, China

Xian-long Meng
Northwestern Polytechnical University
mengxl@nwpu.edu.cn
Xi'an, Shaanxi, China

ABSTRACT

The overall cooling effectiveness(ϕ) is used to provide the actual temperature on the surface of the turbine vane, which is measured using IR thermography with high resolution and dynamic range in current study. The effects of geometrical parameters of turbine vane leading edge on ϕ are experimentally and numerically investigated. Three specimens of turbine vanes are investigated including two wall thicknesses (2.28mm,5.7mm) and two film cooling hole diameters (0.95mm,0.66mm). In addition, the total areas of the film holes outlets for specimens are the same to ensure similar flow resistance characteristics. The experiments are modelled in a low-temperature state(T_g=583K, T_c=293K). The mainstream Reynold number (Re_g) is 165,000, and four typical mass flow ratios (*MFR*) are designed, 0.35%, 0.52%, 0.69% and 1.02%. Results show that: the hole diameter plays a pivotal role on ϕ distirbution. Two vanes with smaller diameter of film hole have higer overall cooling effectiveness than the model with larger diameter at all *MFR* conditions. The ϕ distributions are nonhomogeneous along the streamwise and lateral direction, especially at low *MFR* conditions for three vanes. This is mainly caused by the uneven coolant flow distribution at low MFR. However, the ϕ distribution will be more uniform as the *MFR* increases due to the denser coolant outflow at each hole row. Furthermore, the influence of wall thicknesses on ϕ is different as *MFR* increases from 0.35% to 1.02%, and the ϕ of thicker wall model has a greater increase.

1 INTRODUCTION

With the demand for higher performance aeroengines, the turbine inlet temperature is getting higher[1], which puts forward higher requirements on the cooling technology of the turbine vanes. The leading edge of turbine vane is the focused region with the largest heat load due to the direct impact of high-temperature gas, so it is easy to produce ablation phenomenon and cannot work normally[2]. At present, film cooling technology is mostly used to protect turbine vanes from heating. Therefore, it is particularly important to understand the heat transfer characteristics and cooling effects of the leading edge and downstream region of turbine vanes.

In previous studies, Zhu et al.[3]-[5] conducted a comparative experimental study on the cooling effectiveness of film cooling in the region near the leading edge under different number of holes and different positions of holes, including three kinds of single row hole position, three kinds of two row hole position and one kind of three row hole position. The results showed that the hole arrangement has little effect on the downstream cooling effectiveness at large secondary flow rate. However, at low *MFR*, the three-row model has better cooling effect, followed by two-row and single-row model. Ravell and Barigozzi[6] evaluated the cooling performance of the vane leading edge by thermochromic liquid crystal technology. The result shows the overall cooling effectiveness is mainly affected by the accumulation of coolant along the direction of the ejection outlet toward the tip, and it is obviously improved as the blowing ratio increase from 2.0 to 3.0. Dyson et al[7] matched the *Biot* number of the leading edge by using high thermal conductivity material to study the effect of film hole spacing on the overall cooling effectiveness. Consequently, when increasing the pitch, the blowing ratio was increased proportionally. Moreover, the increased blowing ratio resulted in increased internal impingement cooling and increased in-

hole convective cooling. The increased internal and convective cooling compensate to some extent for the decreased coolant coverage as the pitch increases. Tan et al[8] measured the leading edge film cooling characteristics of a turbine vane model by infrared camera, and pointed out that when the blowing increase to 1.32, the film cooling effectiveness reaches the highest. Liu et al[9] studied the effect of blowing ratio on the cooling characteristics of leading edge spray in transonic flow. The increase of blowing ratio is beneficial to both suction side and pressure side. However, in the range of blowing ratio 1.7-3.3, the main areas affected by blowing ratio are different. Li et al[10] investigated the influence of aerodynamic parameters such as density ratio on film cooling effectiveness of leading edge. The results showed that the influence of density ratio on film cooling effectiveness is low. At low momentum flux ratio, the average film cooling effectiveness increases with the density ratio, while it shows the opposite law at high momentum flux ratio.

In recent years, with the development of computer technology, the numerical calculation methods to calculate flow heat transfer problems (computational fluid dynamics, *CFD*) has been increasingly used. Rozati and Tafti[11] used the Large Eddy Simulation(*LES*) method to illustrate the effect of the blowing ratio on the leading edge film cooling effectiveness. It was found that the primary entrainment vortex formed on the leeward side of the film hole at low blowing ratio. Moreover, the vortex tube and the typical hairpin vortex of the turbulent boundary layer produced by the vortex tube dominate the flow field. However, when the blowing ratio is 0.8 and 1.2, the coherent vortex tube disappears and the strength of the vortex structure is improved, resulting in enhanced turbulent shear between the jet and the mainstream. Thus, the interaction increases significantly as the blowing ratio increases. Sibi Mathew et al.[12] compared the computed results by using realizable k-ε (*KRE*) and shear stress transport k-ω (*SST*) turbulence models It is found that the *RKE* model did not simulate suitable for the leading edge when considering the effects of heat conduction on the solid wall and the impingement of coolant. In addition, the flow separation of coolant in the stagnation region is appropriate by using the *SST* model, while the flow separation in the experiment can not be predicted accurately. Lei et al.[13][14] performed a full three-dimensional Navier-Stokes (*NS*) numerical simulation on the double-row hole film cooling at the cylindrical front edge, and studied the flow mechanism of the jet and the mainstream. In addition, the opposite wall surface under different blowing ratios was analyzed. The calculation results showed that the average adiabatic effectiveness was increases with the increase of the blowing ratio.

So far, the above researches mainly focus on the influence of the arrangement of holes and hole shapes on adiabatic cooling effectiveness and heat transfer. There is rarely research on overall cooling effectiveness. In this paper, we conducted a study on the overall cooling effectiveness of turbine vane leading edge with three cooling structures. The models are magnified by 1.9 times compared with the real turbine vane. The mainstream temperature is 583K, and the Reynolds number based on the vane chord is 165,000. The coolant temperature is 293K. Four coolant mass flow rates(*MFR*) are designed (0.35%, 0.52%, 0.69% and 1.02%). Infrared thermometry method is used to obtain the temperature of the leading edge surface. At the same time, the coolant distribution for three vanes are analyzed by numerical method.

2 METHODOLOGY

2.1 Experimental system

The experimental system consists of the mainstream system, the secondary system, the cascade experimental section and the measurement system, as shown in Figure 1. The mainstream was provided by a high power compressor. The secondary flow was produced from a high-pressure air source. In the meanwhile, the temperature and pressure at cascade section were measured to calculate the air density and Reynolds number, respectively. The surface temperature of vanes were measured by an infrared camera, which was corrected by K-type thermocouples. The calibration thermocouples were buried in the grooves of the leading edge surface. Before the experiment, the black paint was sprayed on the leading edge surface to ensure a high and uniform emissivity. The IR camera monitored the leading edge surface through the ZnS glass observation windows. The transmittance of ZnS glass and other materials varies with wavelength were shown in Figure 2. In the range of 8-14 microns measured by the thermal imager, the transmittance of ZnS glass is stable at about 70%, which was improved to 90% after antireflection.

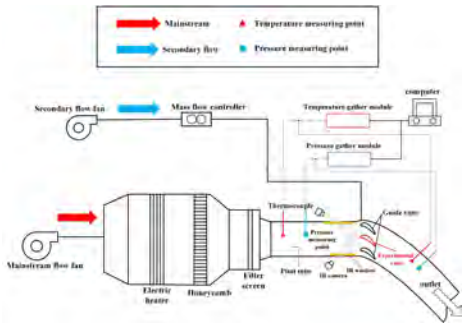

Figure 1 Diagram of experimental system

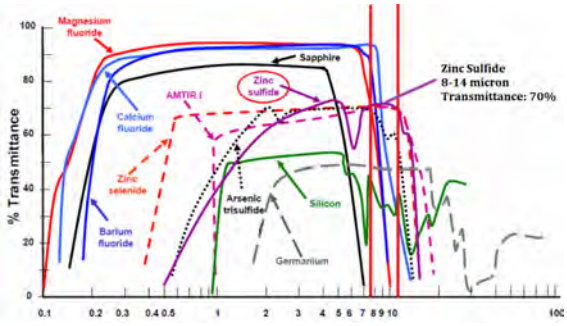

Figure 2 IR window transmittance

Figure 3 shows three vane models with the number of each air film hole row marked. PS1-4 was located in the regions close to the pressure side of the leading edge, SH1-3 was located in the regions near the stagnation line, and SS1-3 was located in the regions close to the suction side. Table 1 shows the experimental conditions.

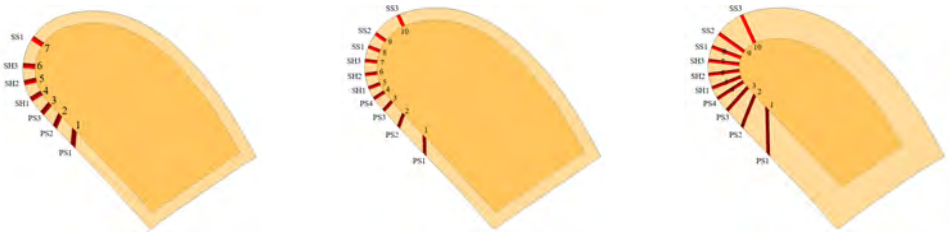

Figure 3 Three vane leading edge structures

Table 1 Experimental conditions

parameters	vane	vane A	vane B	vane C
Geometric	wall thickness	2.28mm	2.28mm	5.7mm
	hole diameter	0.95mm	0.66mm	0.66mm
	vane chord length		C=120mm	
	vane height		H=72.5mm	
Aerodynamic	Re_g		Re_g=165,000	
	T_g		T_g=310℃(583K)	
	MFR		MFR=0.35%, 0.52%, 0.69% and 1.02%	
	T_c		T_c=18-25℃(291-298K)	
	T_g/T_c		T_g/T_c=1.98	

2.2 Numerical method

In this paper, the unstructured grid is divided into fluid domain and solid domain. Interface coupled wall condition was used in the coupling calculation of the composite cooling structure. Figure 4 shows the computational domain. For fluid domain, the *SST* model was used as the turbulence model and $\gamma-\theta$ model was used as the transition model. The scalable wall function is automatically used as the near wall function. This solution setting method was commonly used in the previous turbine vane researches[15]-[17]. The solid domain is controlled by the heat conduction equation. The TC4 titanium alloy was used as the solid domain material, and the polynomial fitting formula of temperature was used for the thermal conductivity and specific heat capacity. High order method was used to solve the convection term in the governing equations. The convergence criterion of the calculation results was that the residual error is less than 10^{-5}, and the average temperature of leading edge surface remain stable within 1000 steps. Figure 5 shows the division of the meshing. Refined grids were adopted at the leading edge of experimental vane, and the boundary layer was divided normal to the leading edge surface in the fluid domain.

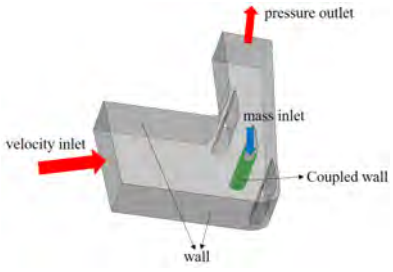

Figure 4 Computational domain

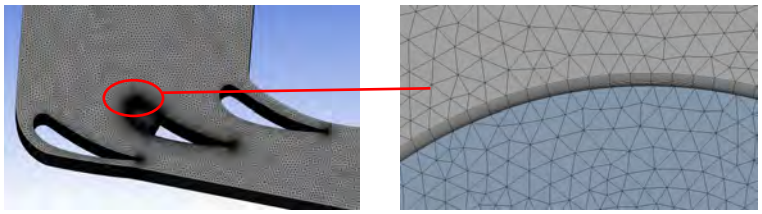

Figure 5 Grids division

3 RESULTS AND DISCUSSION

3.1 Influence of hole diameter

The measured surface temperatures of the two infrared observation windows are respectively flattened. The X-axis is the ratio of the leading edge arc length to the vane chord length(S/C), and S/C=0 represents the leading edge stagnation line located. S/C<0 represents the pressure side, and S/C>0 represents the suction side. The Y-axis is the ratio of the height to the chord length(H/C), and H/C=0 represents the location on section side of 50% height, that is, the junction of holes with opposite inject angles. The 10mm from the top and bottom of the 50% section of the vane height were selected as the research and analysis object.

Figure 6 is a set of contour diagrams of the overall cooling effectiveness of vane A and B at different *MFRs*. The first and second rows show the measured ϕ distributions of vane A and vane B, respectively. In each diagram, four specific positions are selected from the PS to the SS side to mark it. The direction of coolant flow into the chamber is from top to bottom. The overall cooling effectiveness(ϕ) for both vanes increases with the *MFR* increases. However, the rise characteristics and the ϕ distribution are different. At low *MFR*, the ϕ of vane A arranged less film holes with large diameters is more evenly distributed along streamwise and lateral direction than vane B, which was arranged more film holes with small diameters. The ϕ on suction side of leading edge is significantly larger than pressure side for vane B. Meanwhile the ϕ of upper region is obviously larger than that of the lower region. However, the difference is not apparent for vane A. As the *MFR* increases, the ϕ on pressure side of leading edge for both vanes are significantly improved. Also the cooling effectiveness of the lower region of vane B is also improved. But the value on suction side does not change obviously for both vanes. Therefore, the situation here has reversed. The ϕ for vane B is more uniform than that for vane A, and the value of ϕ is also higher than vane A on the whole regions.

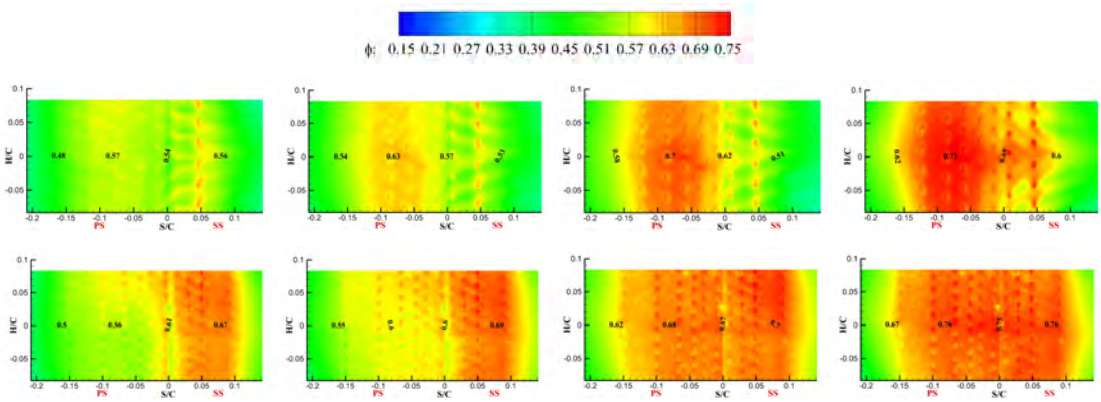

Figure 6 Overall cooling effectiveness contour of vane A and B

Figure 7 is the laterally averaged of ϕ for vane A and B. As mentioned above, the coolant in the chamber is from top to bottom, which leads to uneven distribution of pressure for coolant before outflowing through the holes. Moreover, it is obvious to find that the mainstream pressure at pressure side of leading edge is higher than suction side. Consequently, the distribution of ϕ on the pressure side of leading edge at low *MFR* is uneven owing to the unequal mass flow and pressure distribution. Several factors may contribute to this phenomenon. Firstly, the coolant pressure in the chamber decreases along the streamwise direction. The outflow through film holes on the vane surface decreases along this direction, thus it is harder for coolant to flow through the holes and far away from the inlet. In addition, the heat transfer is occured when the coolant enters the chamber. The cooling capacity of the coolant gradually decreases with the deepening of the flow. This phenomenon will be more distinct due to the insufficient coolant flow. However it will be alleviated when *MFR* further increases. Along the mainstream direction, the overall cooling effectiveness of two vanes are different. The ϕ of pressure side of leading edge is significantly lower than the suction side at low *MFR* for vane B, while it is relatively uniform for vane A at low *MFR*. As the coolant mass flow rate increases, the growth of ϕ on pressure side is much higher than suction side. Therefore, when *MFR* increases to 1.02%, the ϕ on pressure side of leading edge for vane A can reaches to 0.73, while the value on suction side can only reach to 0.65. On the contrary, the ϕ will maintain around 0.74 when *MFR* up to 1.02%.

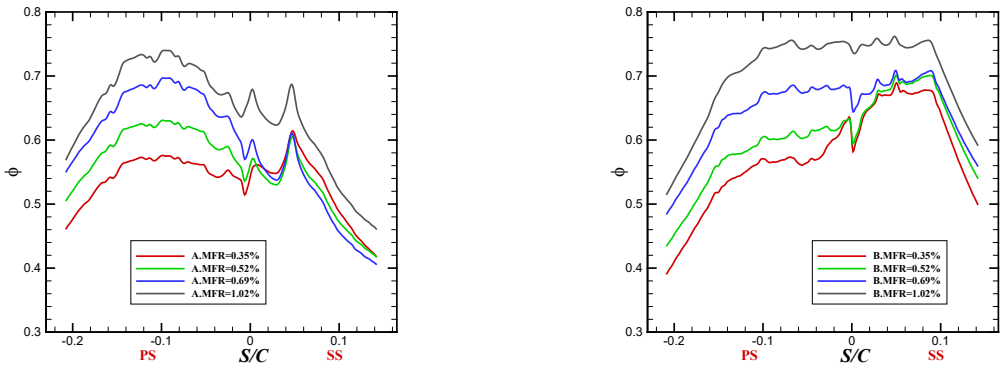

Figure 7 Laterally averaged Φ of vane A and B

Figure 8 shows the streamlines of coolant discharging through the film holes to further analyze the flow characteristic. In each diagram, the coolant discharging through the holes of PS1-PS3 flows to the pressure side surface, while the coolant

discharging through the other rows of holes flow to suction side surface. Although the total area of the whole film holes are the same, the coolant of vane A is more easy to lift-off the wall than vane B at same *MFR*. This can be interpreted that the coolant outflow of each hole has a larger contact area with the main stream at larger single hole area. So the coolant flow of vane A is more easily affected by mainstream than vane B. In other words, the coolant is more difficult to attach the downstream surface after outflow. This is a major factor that causing the ϕ of vane A differs from vane B. Along the mainstream flow direction, there are four rows of coolant outflowing to suction side for vane A, while there are seven rows for vane B. Therefore, more coolant flows to suction side of leading edge for vane B, which results in higher ϕ on suction side. In addition, the raise coefficients of coolant mass flow with *MFR* increases for each row of two vanes is different. Table 2 shows the increase of discharge of each row when *MFR* increases from 0.35% to 1.02%. The largest increase for vane A is at PS3 of 342.8%. While the lowest is at SS1 of 58.4%. At the same time, the raise coefficient of ϕ on the pressure side is much larger than suction side, which is approximately 30.4% and 12.1% for vane A and vane B, respectively. However, the largest raise coefficient for vane B is at PS4 of 1050.6%, and the lowest is at SS3 of 34.5%. Meanwhile, the raise coefficient of ϕ on the pressure side and suction side is 36.4% and 11.9%, respectively. Based on this, we can find that the raise coefficient of coolant mass flow and overall cooling effectiveness of leading edge pressure side for vane B are higher than vane A. Thus, the distribution of coolant may be an important factor on the distribution of ϕ.

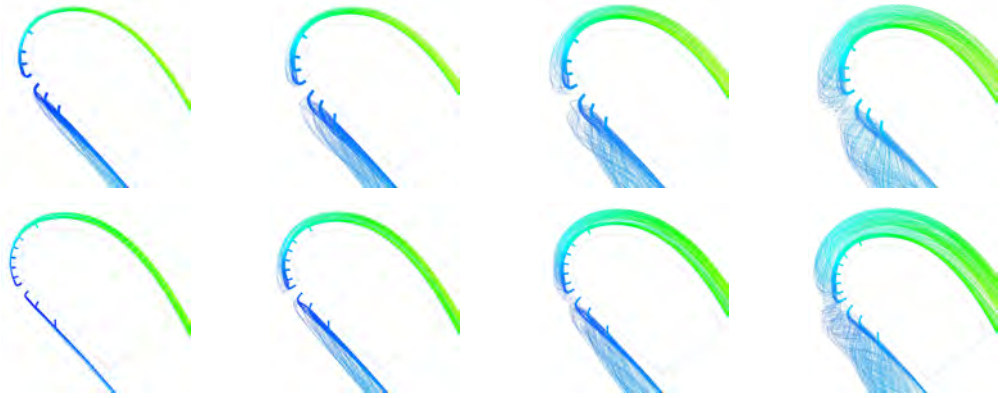

Figure 8 Streamline diagram of vane A and B

Table 2 Increase of coolant outflow of each row

Hole rows	PS1	PS2	PS3	PS4	SH1	SH2	SH3	SS1	SS2	SS3
vane A	298.1%	320.9%	342.8%	---	331.8%	230.8%	136.5%	58.4%	---	---
vane B	555.4%	784.7%	1045.1%	1050.6%	651.7%	314.8%	165.6%	99.8%	60.9%	34.5%

3.2 Influence of wall thickness

Figure 9 shows the contour of ϕ for vane B and C with the increase of *MFR*. The first row is the ϕ of vane B, and the second row is the ϕ of vane C. These two vanes have the similar distribution of overall cooling effectiveness at each *MFR* condition. When the *MFR* is 0.35% and 0.52%, the vane B has an uneven distribution as described above, and the vane C has the similar distribution as vane B due to the same reason. When further increase the *MFR*, the coolant flow becomes more equal through each hole along the vane height direction, the ϕ on the pressure side of leading edge has more growth than the suction side, thus the distribution of ϕ becomes more uniform. The value of overall cooling effectiveness for vane C is lower than vane B, especially at *MFR*<1%. However, with the *MFR* increases, the value of ϕ for vane C is closer to vane B. The difference between them is gradually narrowing.

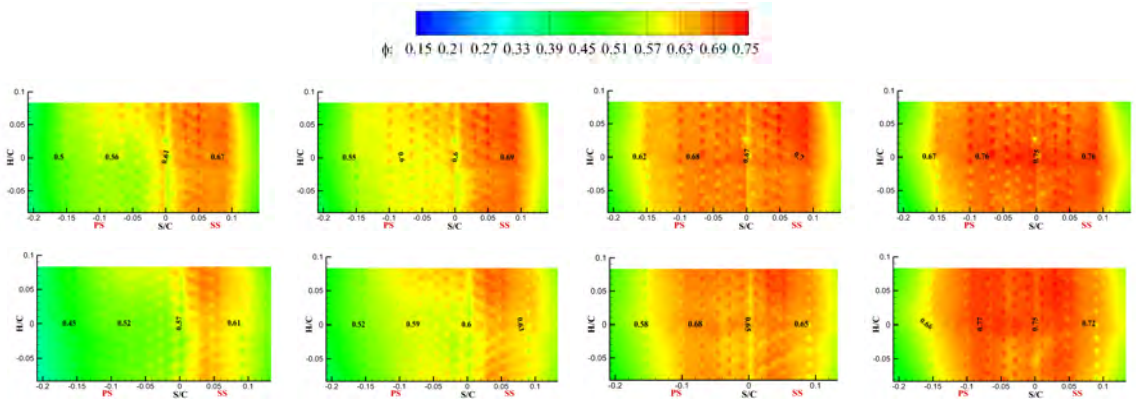

Figure 9 Overall cooling effectiveness contour of vane B and C

Figure 10 shows the laterally averaged distribution of ϕ for vane B and C. The two vanes show the similar characristics in both distribution and value. It can be seen that the ϕ on the pressure side of leading edge is lower than that on suction side at the low *MFR*. Then the distribution tends to be uniform when the *MFR* increases.

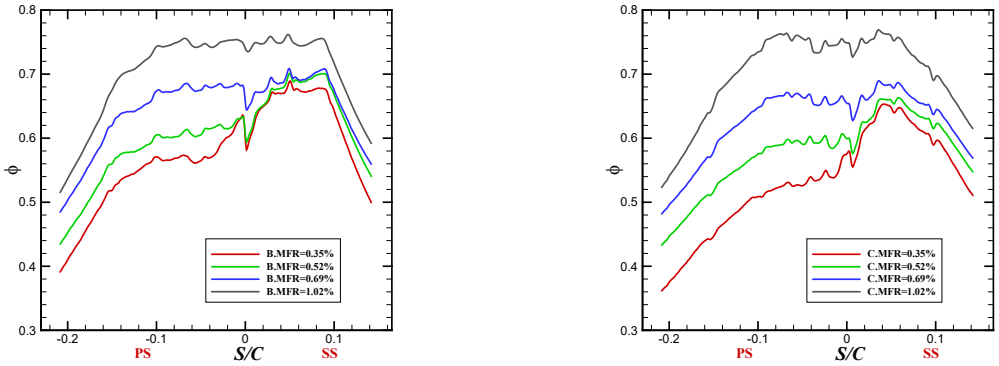

Figure 10 Laterally averaged Φ of vane B and C

Since the hole layout of vane B and C is the same, figure 11 shows the flow distribution of the two vanes. In the case of low *MFR*, the discharge flow of each hole is different. Most of the coolant out of the suction side, which leads to the cooling effect on the suction side is much higher than that of the pressure side. When the *MFR* increases, the coolant flow increases more at the pressure side, so the difference of discharge flow of each hole decreases gradually. Cause the minimum flow out of each vane is at PS1 hole and the maximum is at SS3 hole, other holes are between them. So the relative difference between outlet flow of SS3 hole and PS1 hole can reflect the distribution of coolant flow of two structures to a certain extent.

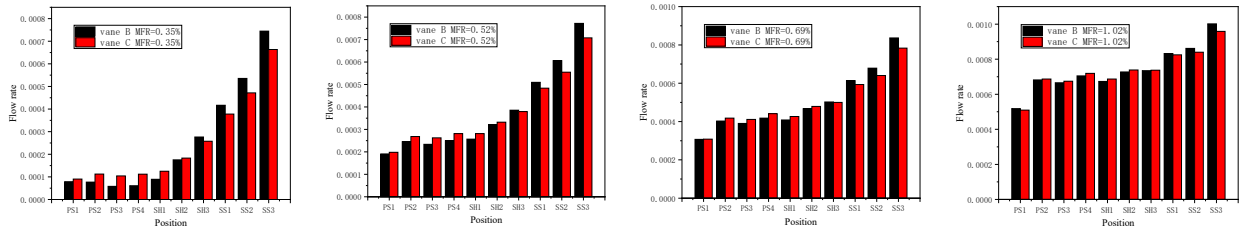

Figure 11 Second flow distribution of vane B and C

Table 3 shows the raise coefficient of the coolant flow rate at each row from the minimum to the maximum *MFR* for vane B and C. The raise coefficients on the pressure side are much larger than suction side for both vanes, but the values for two vanes are different in specific. The vane B has a larger increase on the pressure side of leading edge. The coolant outflow through PS4 is increased 1050.6% for vane B, but it is increased only 543.5% for vane C. However, the coolant outflow through SS2 is increased 60.9% for vane B, but it can be increase 78.0% for vane C. This is because the outflow of each row of vane B has larger difference than vane C at low *MFR*, and it becomes denser as the *MFR* increases.

Table 3 Increase of coolant outflow for vane B and C

Hole rows	PS1	PS2	PS3	PS4	SH1	SH2	SH3	SS1	SS2	SS3
vane B	555.4%	784.7%	1045.1%	1050.6%	651.7%	314.8%	165.6%	99.8%	60.9%	34.5%
vane C	463.9%	510.9%	546.5%	543.5%	448.8%	303.5%	186.0%	118.2%	78.0%	44.4%

3.3 Area averaged ϕ comparison

In order to further compare the advantages of different structures, we propose the area average of the overall cooling effectiveness, $\overline{\phi}$. It is obtained by the formula:

$$\overline{\phi} = \frac{\sum_{i=1}^{m}\sum_{j=1}^{n}\phi_{i,j}}{m \times n} \tag{1}$$

Figure 12 shows the variation of the area averaged $\overline{\phi}$ of the leading edge region for three turbine vanes. The value of $\overline{\phi}$ is improved for three vanes with the *MFR* increases. In specific, the vane A and vane B have the same wall thickness, but different hole diameters. The area averaged $\overline{\phi}$ for the two vanes have similar growth trend but different values. On the contrary, the vane B and C have the same hole diameter but different wall thicknesses. This may lead to different raise coefficients of $\overline{\phi}$. The value of $\overline{\phi}$ for vane C at low *MFR* is closer to vane A, but it has a faster growth rate. When the MFR

has reached to 1.02%, the value of $\bar{\phi}$ for vane C is nearly as same as vane B. Therefore, we can infer that: the smaller hole can lead to high overall cooling effectiveness and the thicker wall has a faster growth of $\bar{\phi}$ with the *MFR* increases.

In turbine vane cooling technology, the uniform temperature distribution on the mainstream side of vane is also significant besides high overall cooling effectiveness. Herein, we propose Relative Standard Deviation(*RSD*)[18] to evaluate the uniformity of overall cooling effectiveness. The formula of *RSD* is as follows:

$$RSD = \frac{S}{\bar{\phi}} \times 100\% = \frac{\sqrt{\frac{\sum_{i=1}^{n}(\phi_i - \bar{\phi})^2}{n-1}}}{\bar{\phi}} \times 100\% \tag{2}$$

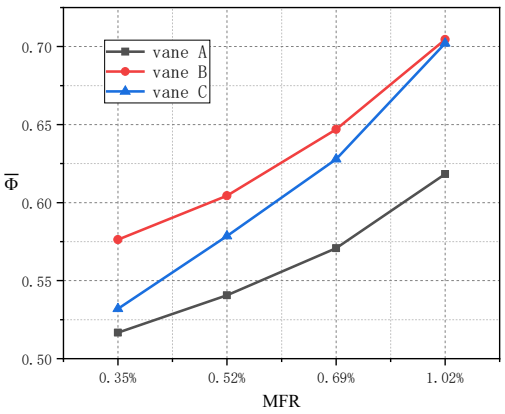

Figure 12 Area averaged ϕ

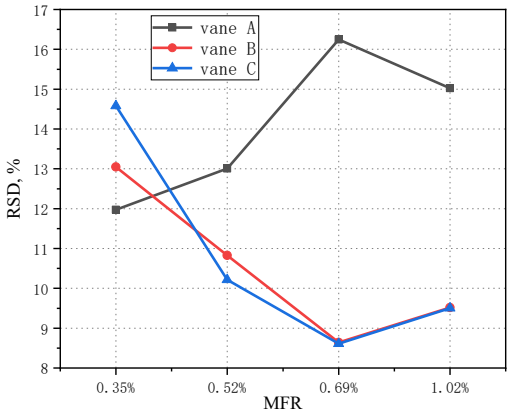

Figure 13 *RSD* value of ϕ

in which *S* is the standard deviation(also can be expressed as *SD*), $\bar{\phi}$ is the area averaged overall cooling effectiveness. The lower value of *RSD* means more uniform distribution of overall cooling effectiveness. As shown in figure 13, the vane A has the most uniform distribution as the *MFR* is at 0.35%, then followed by vane B and C. However, when the *MFR* increases, the distribution of vane A begins to become uneven mainly because the ϕ on pressure side is higher than suction side. The *RSD* value can rise to around 16% when the *MFR* is at 0.69%. Contrary to vane A, the values of ϕ on pressure side and suction side of leading edge for vane B and C become equal when the *MFR* increases. Thus the *RSD* drops below 10% when the *MFR* is at 0.69%. In addition, the *RSD* value for vane A has a slight drop and that for vane B and C has a slight rise when the *MFR* increases to 1.02%, but it is little change generally.

CONCLUSIONS

In this paper, the experiments and numerical simulation were performed to analyze the effects of geometric parameters on the overall cooling effectiveness of the leading edge of three turbine vanes. The vanes were made of the titanium alloy with high thermal conductivity. The temperature ratio between mainstream and coolant maintains at 1.9 for simulating the real engine conditions. The mainstream Reynolds number is 165,000. The coolant mass flow ratio ranges from 0.35%-1.02%. The temperature of the leading edge surface is obtained by using the infrared thermal imager corrected by thermocouples. Combined with numerical method, the differences of overall cooling effectiveness distribution among three vanes are explained from the coolant flow distribution of each hole row. Finally, we proposed *RSD* to evaluate the uniformity of ϕ on leading edge. The conclusions are as follows:

(1)The overall cooling effectiveness of the three vanes increases as the *MFR* increases. Vane B and C with small film holes have higher ϕ than vane A with large holes at each *MFR*. Vane B with thin wall has higher ϕ than vane C with thick wall at lower *MFR*s, but vane C has higher raise coefficient as the *MFR* increases. Meanwhile, vane A and B with thin wall have similar regulation of ϕ. When the *MFR* increases from 0.35% to 1.02%, the raise coefficient of ϕ for vane A, B and C is 19.7%, 22.3% and 32.0%, respectively. Therefore, when the *MFR* is constant, the vanes with small holes have higher overall cooling effectiveness. When the *MFR* increases, the wall thickness plays a more significant role on the overall cooling effectiveness.

(2)The coolant discharging has greatly contributed to the distribution of overall cooling effectiveness for three vanes. The coolant tends to outflow through the holes at upper region and suction side of leading edge at low *MFRs* especially for vane B and C. Hence the ϕ at upper region and suction side is significantly higher than other regions. But the ϕ distribution for vane A at low *MFRs* is relatively uniform due to large and less film holes, which may result in the closely average distribution of coolant. However, more coolant will flow to the holes at bottom region and pressure side as the *MFR* increases. The coolant distribution tends to be more average. Thus the distribution of ϕ becomes more uniform especially for vane B and C. But for vane A, cause the ϕ of both sides is close at the low *MFR*. Therefore the ϕ on pressure side of leading edge becomes larger than suction side.

NOMENCLATURE

d	Diameter of film cooling hole	l	Film cooling hole length
t	Wall thickness of leading edge	C	Vane chord length
S	Arc length of leading edge	H	Vane height
Re_g	Reynolds number of mainstream	Re_c	Reynolds number of coolant flow
T_g	Temperature of mainstream	T_c	Temperature of coolant flow
Bi	Biot number, ht/λ	Φ	Overall cooling effectiveness
TC	Thermocouple	IR	Infrared camera
PS	Pressure side of leading edge	SS	Suction side of leading edge
MFR	Mass flow ratio of coolant to mainstream	RSD	Relative Standard Deviation

ACKNOWLEDGMENTS

The authors acknowledge gratefully the financial support from National Science and Technology Major Project（2017-III-0001-0025).

REFERENCES

[1] R. J. Goldstein. Film Cooling[J]. Advances in Heat Transfer, 1971, 7: 321~379.

[2] D. M. Kercher. Turbine Airfoil Leading Edge Film Cooling Bibliography: 1972~1998[J]. International Journal of Rotating Machinery, 2000, 6(5): 313~319.

[3] ZHU Hui-ren, XU Du-chun, GUO Tao, et al. An experimental investigation of film cooling effectiveness on leading edge of turbine blade[J]. Journal of Aerospace Power, 1999,14(2):205-208,223-224.

[4] ZHU Hui-ren, XU Du-chun, GUO Tao, et al. Experimental investigation of film cooling heat transfer on turbine blade leading edge[J]. Journal of Propulsion Technology, 1999,20(2):64-68.

[5] ZHU Hui-ren, XU Du-chun, GUO Tao, LIU Song-ling. et al. Influences of position of hole-rows on film cooling on leading edge of turbine blade[J]. Acta Aeronautica et Astronautica Sinica, 2000,21(5):385-388.

[6] Ravelli S, Barigozzi G. Comparison of RANS and detached eddy simulation modeling against measurements of leading edge film cooling on a first-stage vane[J]. Journal of Turbomachinery, 2017, 139(5):051005.

[7] Thomas E. Dyson, D. G. Bogard, Justin D. Piggush, Atul Kohli. Overall Effectiveness for a Film Cooled Turbine Blade Leading Edge With Varying Hole Pitch[J]. Journal of Turbomachinery, 2013.

[8] TAN Xiao-ming, ZHU Xing-dan, GUO Wen, Et al. Heat transfer experiment on film cooling of turbine blade leading edge[J]. Journal of Aerospace Power, 2014,29(11):2672-2678.

[9] Liu C L, Zhu H R, Fu Z Y, et al. The effects of inlet Reynolds number, exit mach number and incidence angle on leading edge film cooling effectiveness of a turbine blade in a linear transonic cascade[R]. ASME paper, 2015, No. GT2015-42888.

[10] LI Guang-chao, ZHU Hui-ren, LIAO Nai-bing, et al. Influence of aerodynamic parameters on film cooling effectiveness on the xane leading edge[J]. Journal of Aerospace Power, 2008,23(2):215-220.

[11] Rozati A, Tafti D K, Effect of coolant–mainstream blowing ratio on leading edge film cooling flow and heat transfer-LES investigation[J]. International Journal of Heat and Fluid Flow, 2008, 29(4):857-873.

[12] Sibi Mathew, S.R., David G. Bogard, Evaluation of CFD Predictions Using Thermal Field Measurements on a Simulated Film Cooled Turbine Blade Leading Edge. Journal of Turbomachinery, 2013.

[13] LEI Yun-tao, LIN Zhi-rong, YUAN Xin. Numerical simulation of film cooling at the leading edge of a turbine blade with two rows of staggered holes[J]. Journal of Tsinghua University(Science and Technology), 2010,50(11):1843-1847.

[14] LEI Yun-tao, YUAN Xin, Numerical simulation on the effect of film cooling at leading edge of turbine blade with two rows of staggered holes[J]. Journal of Propulsion Technology, 2012,33(5):704-709,770.

[15] LIU Cong, ZHU Hui-ren, XU Wei-jiang, et al. Numerical study on heat transfer characteristics of suction side of transonic turbine guide vanes. Journal of Propulsion Technology, 2015, 36(7):1046-1053.

[16] Arts T, Duboue J M, Rollin G. Aerothermal Performance Measurements and Analysis of a Two-Dimensional High Turning Rotor Bladee. Journal of Turbomachinery，1998, 1998, 120: 494-499.

[17] Giel P W, Boyle R J, Bunker R S. Measurements and Predictions of Heat Transfer on Rotor Blades in a Transonic Turbine Cascade. Journal of Turbomachinery, 2004, 126: 110-121.

[18] Jiang, Hongde, Li, et al. Effect of Reynolds Number, Hole Patterns, and Target Plate Thickness on the Cooling Performance of an Impinging Jet Array-Part II: Conjugate Heat Transfer Results and Optimization[J]. Journal of Turbomachinery, 2017.